Penetration of spheres into loose granular media

John R. de Bruyn and Amanda M. Walsh

Abstract: We study the penetration of steel spheres dropped vertically into a container of loosely packed, small glass beads. We find that the penetration depth of the spheres increases linearly with the incident momentum of the projectile, but with a zero-momentum intercept that can be either positive or negative. This behavior can be understood by modelling the granular medium as a non-Newtonian fluid with a yield stress and an effective viscosity. We derive the scaling behavior of the viscosity and find agreement with our experimental results.

PACS Nos.: 45.70.–n, 83.80.Fg, 47.50.+d

Résumé : Nous étudions la pénétration de billes d'acier tombant verticalement dans un récipient contenant de la fine grenaille de verre. Nous observons que la pénétration augmente linéairement avec la quantité de mouvement du projectile, mais avec une valeur à l'origine non nulle qui peut être positive ou négative. Ce comportement peut se comprendre en modélisant le milieu comme un fluide non-Newtonien avec un effort d'écoulement et une viscosité efficace. Nous obtenons ici le bon comportement d'échelle de la viscosité et un bon accord avec les données expérimentales.

[Traduit par la Rédaction]

1. Introduction

Granular media exhibit a range of complex behavior and can have properties ranging from solid-like to gas-like [1–3]. They also have innumerable applications — much of the World's economic activity involves the production, processing, and transport of granular materials. For these reasons, these materials have been the subject of substantial study. Of particular interest is the transmission of forces by and through granular materials. In a static granular medium, force chains involving a series of point contacts between individual particles arise [4]. A particle moving through the material experiences a drag force that results from the integrated effect of these chains [5]. The configuration of the force chains changes as the particle moves, so the net force varies in a complicated manner with time [6]. For slow motion of objects of lateral dimension D through a granular medium, Schiffer et al. [5] found a drag force that was independent of velocity v, proportional to D, and increased quadratically with depth. For a sphere moving through a granular material fluidized by vibration, Zik et al. [7] measured a drag force proportional to v, so the material behaved like a fluid with an effective viscosity that depended

Received 5 February 2004. Accepted 15 April 2004. Published on the NRC Research Press Web site at http://cjp.nrc.ca/ on 3 June 2004.

J.R. de Bruyn[1,2] and A.M. Walsh. Department of Physics and Physical Oceanography, Memorial University of Newfoundland, St. John's, NF A1B 3X7, Canada.

[1]Corresponding author (e-mail: jdebruyn@physics.mun.ca).
[2]Also at: Laboratoire de Rhéologie, B.P. 53, Domaine Universitaire, Grenoble 38041 Cedex 9, France.

 doi: 10.1139/P04-025 © 2004 NRC Canada

on depth and vibration frequency. Earlier measurements for rapid motion in fluidized granular media found a drag force that was nonmonotonic in v [8].

In this paper, we report measurements of the penetration of steel balls impacting on targets of loosely packed glass beads. We interpret our results in terms of an effective viscous drag exerted on the balls by the fluidized granular medium. The penetration of objects into granular media has recently been studied experimentally [9–11] and numerically [11]. Uehara et al. [9] dropped spheres of different sizes and densities vertically into glass beads and other granular targets. Newhall and Durian [10] extended this work to include objects of different shapes. In both cases the depth of penetration δ was found to be proportional to $H^{1/3}$, where H is the total distance traveled by the projectile. This scaling could not be explained in terms of either a v-independent stopping force or a viscous drag. Ciamarra et al. [11] performed experiments and simulations on granular impacts in a two-dimensional system. They found both the mean force on the projectile and δ to be proportional to the impact velocity v_0. While our data are, in general, consistent with those of ref. 9, they do not obey the scaling suggested in that work. We find, however, that both our results and those of ref. 9 can be understood by modeling the granular material as a viscous fluid with a yield stress. This model is also consistent with the two-dimensional results of ref. 11.

2. Experiment

Our experimental apparatus was the same as that used in ref. 12 to study the formation of impact craters in granular materials. Before each trial, spherical glass beads of a particular size were poured into a container 19 cm deep and 23 cm in diameter. Five bead sizes were used: 45–90, 75–125, 125–180, 180–250, and 300−425 μm. The two smaller sized beads were poured through a sieve to prevent clumping, although the 45−90 μm beads remained slightly cohesive [12]. Except for smoothing the surface with a straight edge, the beads were used as poured, with no shaking. From measurements of the mass and volume of smaller samples of our glass beads prepared in the same way, we determined the packing fraction p of the target materials to be between 56% for the smallest beads (close to that for random loose packing) up to 62% for the largest. Steel balls with diameters $D_B = 2.54$ and 1.27 cm, with masses $m = 66.0$ and 8.35 g, respectively, were dropped into the target using a release mechanism. The release height, h, was measured from the surface of the beads to the lower surface of the steel ball, i.e., h is the distance the ball falls under the influence of gravity before it makes contact with the target. The velocity of the ball at impact v_0 is determined from the release height of our projectiles: $v_0 = \sqrt{2gh}$, with g the acceleration due to gravity. In most cases the projectile was completely buried in the target material after impact, and δ, defined as the distance from the level of the original surface of the target material to the bottom of the ball, was determined by inserting a probe into the beads and locating the top of the ball. δ is the distance over which the ball interacts with the granular medium, and is thus a measure of the average force exerted by the medium on the ball [9].

3. Results and discussion

Figure 1 shows our results for δ plotted as a function of the momentum of the sphere at impact, mv_0. Data for both balls and all five grain sizes are shown. All of the data sets fall on straight lines, but with significantly nonzero δ intercepts. Fits to two data sets are shown as dotted lines; the other fits are omitted for clarity. One of the fits shown has a positive intercept δ_0, while the other has a negative intercept.

Except for the nonzero intercept, this behavior is similar to that of a sphere of radius r moving slowly through a viscous fluid in the absence of gravity. The sphere will experience a drag force described by Stokes' law,

$$F_d = -6\pi\eta r v \tag{1}$$

© 2004 NRC Canada

Fig. 1. The penetration of steel balls into a target of loosely packed glass beads as a function of the incident momentum. Open symbols are for a ball with diameter $D_B = 1.27$ cm and solid symbols are for $D_B = 2.54$ cm. The different symbols indicate different bead diameters, D_g: circles, 300–425 μm; upward triangles, 180–250 μm; squares, 125–180 μm; downward triangles, 75–125 μm; and diamonds, 45–90 μm. The dotted lines are straight line fits to the data for $D_B = 2.54$ cm, $D_g = 300$–425 μm and for $D_B = 1.27$ cm, $D_g = 45$–90μm.

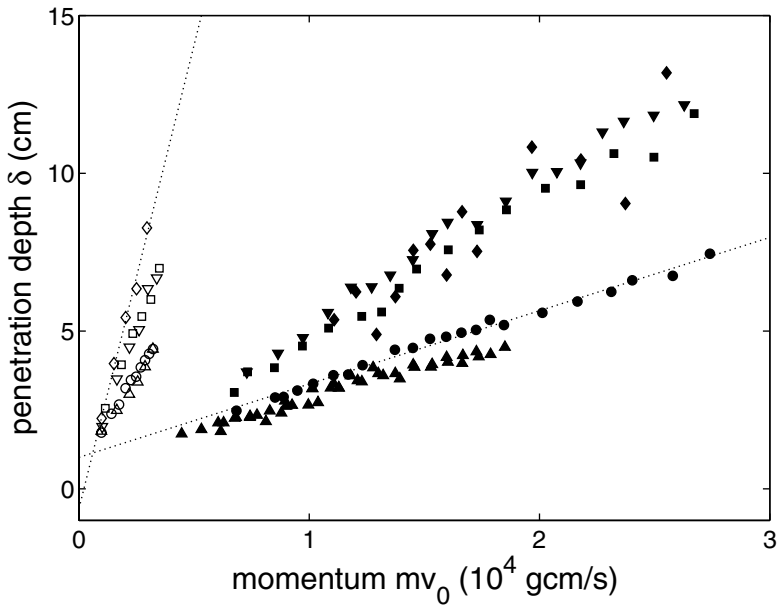

where η is the fluid's viscosity, and the ball will penetrate to depth $\delta = mv_0/6\pi\eta r$. The penetration depth is thus proportional to the momentum of the ball at impact and inversely proportional to the viscosity. By analogy, this suggests that the slopes of the straight lines fit to the data plotted in Fig. 1 should be inversely proportional ηD_B, where η is now an effective viscosity of the granular medium. Although for a Newtonian fluid the viscosity is a property of the material, Fig. 1 indicates that the effective viscosity of the granular medium studied here depends on both D_B and the properties of the granular medium.

To explain our results, we model the granular medium as a Bingham fluid, that is, a fluid with a yield stress and an effective viscosity. If the applied stress is less than the yield stress, such a material behaves as an elastic solid, but for stresses larger than the yield stress it flows. We further assume that the drag force due to the viscosity is Stokes-like, that is, that it is linear in v. In the presence of gravity, a sphere falling through a Newtonian fluid (with no yield stress) will reach a terminal velocity when mg and the drag force balance. In the present case, the ball ultimately comes to rest because the material has a yield stress that is large enough to support the ball against gravity. We, therefore, write the net force on the moving ball as

$$F_d = -F_0 - kv \tag{2}$$

where $F_0 = F_1 \mathrm{sgn}(v)$ is the net force due to the yield stress (i.e., for $v > 0$ it is the total force due to the yield stress less mg). F_0 changes sign when the direction of motion changes, and is zero when the ball is at rest. We take the magnitude of this force, F_1, to be a constant. The second term on the right-hand side is the effective viscous drag, with $k \propto \eta D_B$. By integrating (2) and finding the time at which $v = 0$, we get a penetration depth δ in this model given by

$$\delta = \frac{mv_0}{k} - \frac{F_0 m}{k^2} \ln\left(1 + \frac{v_0 k}{F_0}\right) \tag{3}$$

© 2004 NRC Canada

The first term on the right-hand side is proportional to the incident momentum of the sphere and inversely proportional to the viscosity, as for a Newtonian fluid in the absence of gravity. The second term is due to the yield stress. If $v_0 k/F_0 \ll 1$ (i.e., if the yield stress is large enough or the impact velocity small enough), then $\ln(1 + v_0 k/F_0) \approx v_0 k/F_0$, and the penetration is zero. On the other hand, if $F_0 = 0$ the logarithmic term vanishes and we recover the Newtonian result. For large enough v_0, the logarithmic correction varies slowly with v_0 and a plot of δ versus mv_0 would look like a straight line with an intercept $\delta_0 < 0$.

Unlike the case for a Newtonian fluid, the resistance of a granular medium to flow will depend on both the properties of the medium itself and the imposed flow conditions. A very loose material, for example, would be expected to have lower effective viscosity than a more tightly packed material. With this in mind, we can derive the scaling behavior of η from the definition of viscosity,

$$\eta = \sigma / (\partial v_z / \partial r) \tag{4}$$

where σ is the shear stress, v_z is the flow velocity in the z (vertically downward) direction, and $\partial v_z/\partial r$ the shear rate in the fluidized granular target in cylindrical coordinates.

The shear stress is the force due to the shear divided by the area over which it acts. The force exerted by the granular medium on the ball is typically $mgh/\delta \sim g\rho_B D_B^3 h/\delta$, where ρ_B is the density of the ball. The area is of the order of the surface area of the ball, which is proportional to D_B^2, so the stress is $\sigma \sim g\rho_B D_B h/\delta$.

The velocity of the ball at impact is $(2gh)^{1/2}$. Assuming that the energy of the projectile is transferred elastically to the motion of the grains on impact, we get a typical granular velocity of $v_z \sim v_0 \left(\rho_B/\rho_g\right)^{1/2} \sim \left(gh\rho_B/\rho_g\right)^{1/2}$, where ρ_g is the bulk density of the granular medium. It is known that the velocity field around a sphere moving through a yield-stress fluid drops to zero over a distance of order D_B [13, 14], so the shear rate is given by $\partial v_z/\partial r \sim v_z/D_B \sim \left(g\rho_B h/\rho_g D_B^2\right)^{1/2}$. Neglecting numerical factors, inserting these results into (4) gives

$$\eta \sim g^{1/2}(\rho_B \rho_g)^{1/2} D_B^2 h^{1/2}/\delta \tag{5}$$

We still have to deal with the term $h^{1/2}/\delta$ in (5). This term is proportional to the reciprocal of the slopes of the data sets plotted in Fig. 1. Figure 1 shows that $h^{1/2}/\delta$ is constant for a given projectile and target, but varies with both projectile size and the nature of the target material. This quantity has dimensions $(\text{length})^{-1/2}$. Since in our model the granular material acts as a continuum, the size of the beads cannot matter, and the only relevant length scale in the problem is the diameter of the projectile, D_B. We, thus, expect $h^{1/2}/\delta \sim D_B^{-1/2}$. (This term could, in principle, also involve a factor of ρ_B/ρ_g to some power, since the dimensions would remain correct. We assume here that all of the density dependence has been accounted for, an assumption that is justified by comparison with the experimental results.) Using this in (5) gives[3]

$$\eta \sim g^{1/2}(\rho_B \rho_g)^{1/2} D_B^{3/2} \tag{6}$$

This indicates that η indeed depends on D_B, in contrast to the Newtonian viscosity. Qualitatively, this is because moving a larger and larger object through a granular medium requires physically displacing more and more grains; the number of grains to be displaced and the work required to displace them increases faster than linearly with the size of the object.

[3]Applying the same reasoning to a Newtonian fluid gives a nonsensical result. This is because, as noted above, the viscosity of a Newtonian fluid is a property of the material and does not depend on the nature of the experiment used to measure it. In the present case, we have assumed the contrary, that is, that the effective viscosity of our granular material is explicitly not a material property but depends on the experimental conditions.

© 2004 NRC Canada

Fig. 2. The slopes of straight lines fit to the penetration depth as a function of the scaled momentum, $mv_0/g^{1/2}(\rho_B\rho_g)^{1/2}D_B^{5/2}$, plotted as a function of the packing fraction p of the granular target material. The dependence on projectile diameter has been scaled out. Open symbols are for a ball with diameter $D_B = 1.27$ cm and solid symbols are for $D_B = 2.54$ cm. The different symbols indicate different bead diameters, D_g: circles, 300–425 μm; upward triangles, 180–250 μm; squares, 125–180 μm; downward triangles, 75–125 μ; and diamonds, 45–90 μm. The broken line is a linear fit that gives an x intercept of $p_c = 0.66 \pm 0.02$.

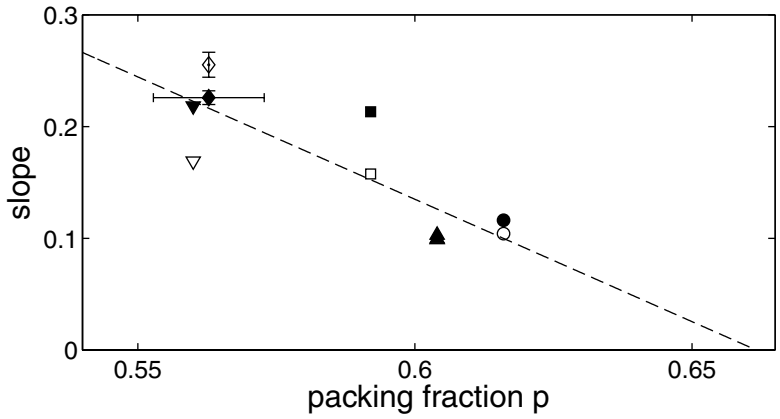

Using this expression for η, (3) gives $\delta - \delta_0 \sim mv_0/k \sim mv_0/g^{1/2}(\rho_B\rho_g)^{1/2}D_B^{5/2}$, where δ_0 is the zero-momentum intercept. An appropriate plot does indeed give a substantial, but not complete, collapse of the data — Fig. 2 is a plot of the slopes obtained using this scaling. There remains, however, a dependence not accounted for by the dimensional analysis given above — the scaled slope decreases as bead size increases. Bead size itself cannot be relevant within our model, since we are treating the granular medium as a continuum. On the other hand, the packing fraction p of the granular target should have an important influence on η via its influence on the shear rate, since it is a measure of the ability of individual particles to move in response to the impact. To show this, we plot the slopes obtained using the above scaling as a function of p in Fig. 2. Figure 2 shows that our $D_B^{5/2}$ scaling has indeed collapsed the data for the two ball sizes. Within the scatter of our data, we can describe the remaining dependence on p by a factor proportional to $1 - p/p_c$, where p_c is the packing fraction at which the effective viscosity becomes infinite. A fit to the data, shown as a broken line in Fig. 2, gives $p_c = 0.66 \pm 0.02$, consistent with the value of 0.64 for random close packing of monodisperse spheres. A value slightly larger than random close packing is not unexpected due to the polydispersity of our glass beads.

Incorporating this packing fraction dependence into our scaling, we plot $\delta - \delta_0$ versus $mv_0(1 - p/p_c)/\left(\mu g^{1/2}(\rho_B\rho_g)^{1/2}D_B^{5/2}\right) = (1 - p/p_c)\left(\rho_B/\rho_g\mu^2\right)^{1/2} D_B^{1/2}h^{1/2}$ in Fig. 3. Here, we have subtracted the zero-momentum intercept from the penetration depth data. μ is a coefficient of friction that will be discussed below. The data collapse reasonably well. All sets have $\delta - \delta_0$ accurately proportional to the scaled momentum, with a mean power-law exponent of 1.01 ± 0.03. The mean constant of proportionality is 1.4 ± 0.3, indicating that the numerical coefficients neglected in our scaling analysis end up, perhaps fortuitously, being of order 1. The variation in this value may be due to inaccuracies in our measurements of the packing fraction.

We also have reanalyzed 21 data sets from similar experiments described in ref. 9. These data are also well-described by our model; that is, δ is linear in mv_0 and the data collapse when plotted as above. Indeed, since ρ_B and ρ_g were not varied in our experiments, we confirmed the predicted density scaling using these data. Fits to these data sets give a mean constant of proportionality of 1.1 ± 0.2, shown as a broken line in Fig. 3. This agrees with the value for our own results within our uncertainty, although differences between the two sets of results due to slight differences in experimental protocol would not

© 2004 NRC Canada

Fig. 3. The penetration depth plotted as a function of the momentum scaled by $\mu g^{1/2}(\rho_B\rho_g)^{1/2}D_B^{5/2}/(1-p/p_c)$, as discussed in the text. Open symbols are for a ball with diameter $D_B = 1.27$ cm and solid symbols are for $D_B = 2.54$ cm. The different symbols indicate different bead diameters, D_g: circles, 300–425 μm; upward triangles, 180–250 μm; squares, 125–180 μm; downward triangles, 75–125 μ; and diamonds, 45–90 μm. The intercept δ_0 has been subtracted. $\delta - \delta_0$ is proportional to the scaled momentum with a mean constant of proportionality of 1.4 ± 0.3. The broken line indicates the mean behavior of the data of ref. 9, with a proportionality constant of 1.1 ± 0.2; the dotted lines show the range of these data.

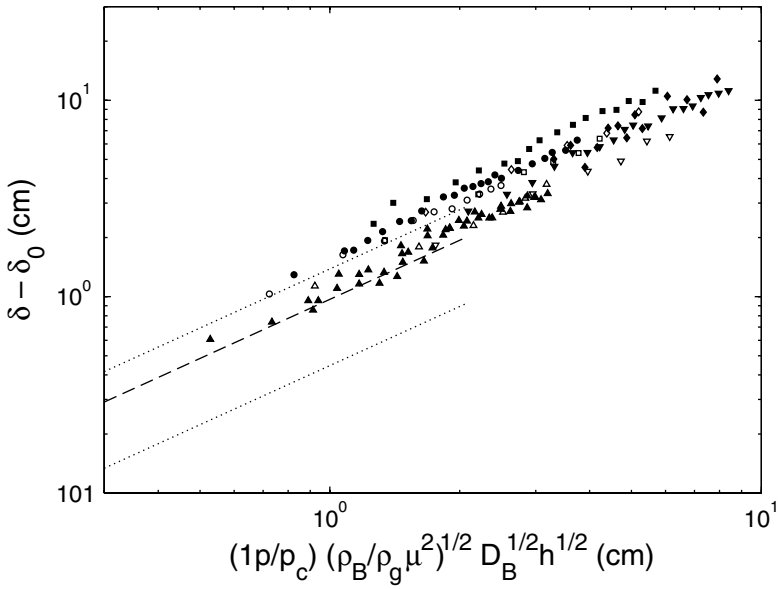

be unexpected. The dotted lines show the range of the fitted data sets. The data of ref. 9 extend from 0.06 to 2.1 on the abscissa of Fig. 3 and overlap with our data over a portion of this range; the upper limit is indicated by the end of the plotted lines. Uehara et al. [9] also found the penetration depth to depend linearly on the friction coefficient $\mu = \tan\theta_r$, where θ_r is the angle of repose of the granular medium [9]. Although θ_r was not accurately measured in our experiments, we have incorporated this dependence into our scaling, assuming $\theta_r = 24°$, the value for the glass beads used in ref. 9.

In previous work [9, 10], the penetration depth data were analyzed in terms of the total change in potential energy of the ball, mgH. Here $H = h + \delta$ is the total distance the ball travels from release to arrest in the target material. δ was found [9, 10] to scale as $(\rho_B/\rho_g\mu^2)^{1/2}D_B^{2/3}H^{1/3}$ for a range of conditions. We test this scaling for our data in Fig. 4. The broken line is the function obtained in ref. 9, with an additional factor of $(1 - p/p_c)$ to account for the packing-fraction dependence noted above (the materials used in ref. 9 all had $p = 0.60$). The data of ref. 9 have values of the quantity plotted on the abscissa in the range from 10^{-1} to 10^3, with the upper limit again indicated by the extent of the broken line, while ours run from 10^2 to 10^4. Our individual data sets fall on straight lines on this log–log plot and collapse rather close to the functional form obtained in ref. 9. Our data do not, however, obey the $H^{1/3}$ power law found in ref. 9. The effective power-law exponents determined from our data are all significantly larger than 1/3 and vary systematically with packing fraction (or bead size) [12]. This is shown in the inset to Fig. 4, where the effective exponent α is plotted as a function of packing fraction. For our largest beads we find $\delta \sim H^\alpha$ with $\alpha \approx 0.4$. As D_g is decreased (p decreased), the exponent increases to $\alpha \approx 0.6$. Note that the inclusion of the packing-fraction term in our scaling improves the collapse of our data, but does not change the values of α.

The logarithmic term in (3) should make a plot of δ versus mv_0 have an apparent intercept $\delta_0 < 0$, while for the most part our data (and those of ref. 9) have $\delta_0 > 0$. This is due to the fact that the

© 2004 NRC Canada

Fig. 4. δ plotted as a function of the total distance traveled H, scaled as described in ref. 9 and in the text. The broken line is proportional to $H^{1/3}$. This line is the function determined in ref. 9 with an additional factor dependent on packing fraction. It ends at the upper limit of the range of their data. Our data do not obey the 1/3 power-law scaling: the inset shows the effective power-law exponents α found from fits of our data to the form $\delta \propto H^{\alpha}$, plotted as a function of packing fraction. Symbols in both the main figure and the inset are as follows: open symbols are for a ball with diameter $D_B = 1.27$ cm and solid symbols are for $D_B = 2.54$ cm. The different symbols indicate different bead diameters, D_g: circles, 300–425 μm; upward triangles, 180–250 μm; squares, 125–180 μm; downward triangles, 75–125 μm; and diamonds, 45–90 μm.

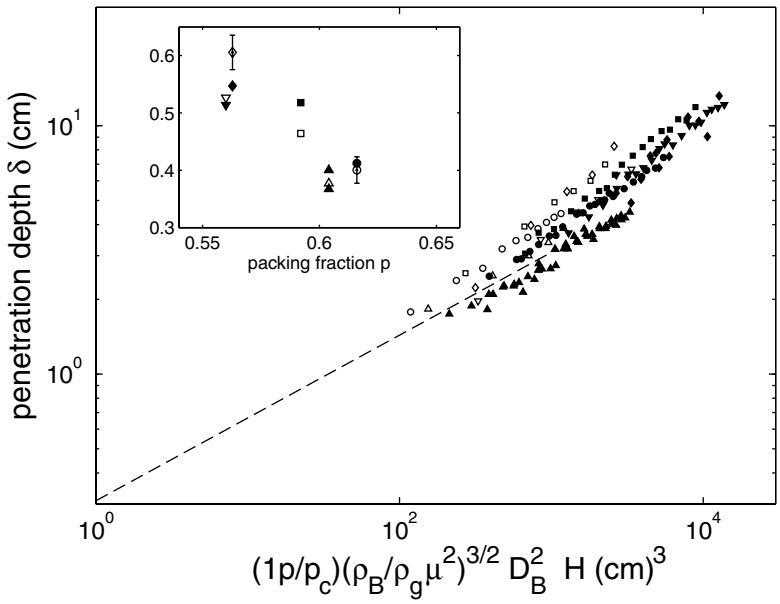

properties of the granular material at the surface differ from those a few grain diameters below the surface. Equation (3) would strictly apply if the sphere was released with an initial speed v_0 in the interior of a homogeneous granular medium. In our case, in contrast, the sphere is released from above the medium. Imagine a ball released from $h = 0$, at which point the bottom of the sphere touches the surface of the target. By our definition, $v_0 = 0$ in this case. However, the sphere does in fact fall some distance into the granular material before coming to a stop, and so has a positive penetration depth at $h = 0$. In terms of the properties of the granular material, the grains near the surface of the target can move much more easily than those beneath the surface, so the yield stress at the surface is substantially lower than in the bulk. As a result the surface layers cannot support the sphere against gravity, and it falls.

One might expect the agreement with the model predictions to improve as the packing fraction decreases, since for loosely packed beads the difference in mobility between beads at the surface and those in the bulk will be less pronounced. Our results for the values of δ_0 are noisy, but the intercept tends to decrease with decreasing packing fraction. For the smallest beads, δ_0 is negative, as shown by one of the fits plotted in Fig. 1, and in agreement with the predictions of (3).

Finally, we note that there is some uncertainty introduced by calculating v_0 on the basis of the distance from the bottom of the sphere at its release point to the surface of the target. As we have seen above, the speed of the sphere can continue to increase even after it has penetrated slightly into the granular material, so the maximum momentum of the ball could be slightly larger than calculated. This would lead to another contribution to δ_0. Calculations indicate that in fact this effect is negligible for our data.

© 2004 NRC Canada

4. Conclusions

In summary, we have observed that the penetration depth of spheres impacting into a granular medium is linearly dependent on the impact momentum, and shown that this behavior can be explained in terms of the yield stress and an effective viscosity of the granular medium. Dimensional analysis and comparison with data indicate that the viscosity is of the form

$$\eta \sim \mu g^{1/2}(\rho_{\mathrm{B}}\rho_{\mathrm{g}})^{1/2} D_{\mathrm{B}}^{3/2}/(1 - p/p_{\mathrm{c}}) \tag{7}$$

We have also analyzed our data in terms of the total change in potential energy of the falling sphere, following the approach of refs. 9 and 10. Our results indicate that the 1/3 power-law exponent found in that work is not universal, but depends on the packing fraction of the granular target material. Our effective viscosity is also not a fixed property of the material, but depends on the dimensions and density of the projectile used in the experiments as well as on the packing fraction, density, and friction coefficient of the granular material. Nonetheless, these results demonstrate an interesting and potentially useful way to characterize a class of granular flows.

Acknowledgements

This research was supported by the Natural Sciences and Engineering Research Council of Canada. J. de B. acknowledges support from CNRS, France. We are grateful to D. Durian for helpful discussions and for making the data of ref. 9 available to us.

References

1. H.M. Jaeger, S.R. Nagel, and R.P. Behringer. Rev. Mod. Phys. **68**, 1259 (1996).
2. J. Duran. Sands, powders, and grains: an introduction to the physics of granular materials. Springer, New York. 2000.
3. G.H. Ristow. Pattern formation in granular materials. Springer, New York. 2000.
4. D.M. Mueth, H.M. Jaeger, and S.R. Nagel. Phys. Rev. E, **57**, 3164 (1998); D. Howell, R.P. Behringer, and C. Veje. Phys. Rev. Lett. **82**, 5241 (1999).
5. R. Albert, M.A. Pfeifer, A.-L. Barabási, and P. Schiffer. Phys. Rev. Lett. **82**, 205 (1998).
6. I. Albert, P. Tegzes, R. Albert, J.G. Sample, A.-L. Barabási, T. Vicsek, B. Kahng, and P. Schiffer. Phys. Rev. E, **64**, 031307 (2001).
7. O. Zik, J. Stavans, and Y. Rabin. Europhys. Lett. **17**, 315 (1992).
8. K. Wieghardt. Annu. Rev. Fluid Mech. **7**, 89 (1975).
9. J.S. Uehara, M.A. Ambroso, R.P. Ojha, and D.J. Durian. Phys. Rev. Lett. **90**, 194301 (2003); Erratum, **91**, 149902 (2003).
10. K.A. Newhall and D.J. Durian. Phys. Rev. E, **68**, 060301 (2003).
11. M.P. Ciamarra, A.H. Lara, A.T. Lee, D.I. Goldman, I. Vishik, and H.L. Swinney. Phys. Rev. Lett. **92**, 194301 (2004).
12. A.M. Walsh, K.E. Holloway, P. Habdas, and J.R. de Bruyn. Phys. Rev. Lett. **91** 104301 (2003).
13. A.N. Beris, J.A. Tsamopoulos, R.C. Armstrong, and R.A. Brown. J. Fluid Mech. **158**, 219 (1985).
14. D.D. Atapattu, R.P. Chhabra, and P.H.T. Uhlherr. J. Non-Newt. Fluid Mech. **38**, 31 (1990).

© 2004 NRC Canada